applied sciences

MDPI

Article

Non-Enzymatic Amperometric Glucose Screen-Printed Sensors Based on Copper and Copper Oxide Particles

Carlota Guati, Lucía Gomez-Coma, Marcos Fallanza and Inmaculada Ortiz *

Chemical and Biomolecular Engineering Department, University of Cantabria, 39005 Santander, Spain; guatic@unican.es (C.G.); lucia.gomezcoma@unican.es (L.G.-C.); marcos.fallanza@unican.es (M.F.)
* Correspondence: inmaculada.ortiz@unican.es

Abstract: Non-enzymatic amperometric glucose sensors have gained much attention in the past decade because of the better chemical and thermal stability and biocompatibility compared to conventional sensors based on the use of biomolecules. This study focuses on a novel copper and copper oxide-based glucose sensor synthesized by an electrodeposition technique through a rigorous protocol which reports an excellent analytical performance due to its structure and its increased active area. In addition, the linear response range, detection limit and sensitivity were 0.5–5.0 mmol L^{-1}, 0.002 mmol L^{-1}, 904 μA $mmol^{-1}$ L^{-1} cm^{-2}, respectively. Results show a reliable electrode as it is chemically stable, exhibits rapid and excellent sensitivity, and it is not significantly affected by coexisting species present in the blood samples; furthermore, it reports a maximum relative standard deviation error (RSD) of 6%, and showed long operating life as the electrode was used for thousand measurements of 4.0 mmol L^{-1} glucose solution during three days.

Keywords: glucose sensor; non-enzymatic; copper oxide; sensitivity

Citation: Guati, C.; Gomez-Coma, L.; Fallanza, M.; Ortiz, I. Non-Enzymatic Amperometric Glucose Screen-Printed Sensors Based on Copper and Copper Oxide Particles. *Appl. Sci.* **2021**, *11*, 10830. https://doi.org/10.3390/app112210830

Academic Editors: Hyeonseok Yoon and Fethi Bedioui

Received: 27 August 2021
Accepted: 11 November 2021
Published: 17 November 2021

1. Introduction

Non-communicable diseases (NCDs), which are not transmissible directly from one person to another, tend to be of long duration and are the result of a combination of genetic, physiological, environmental, and behavioral factors. The main types of NCDs are cardiovascular diseases, cancers, chronic respiratory diseases, and diabetes. According to the United Nations, chronic diseases kill 41 million people each year, equivalent to 71% of all deaths globally. Thus, this organization considers health a fundamental right for human and sustainable development as non-communicable diseases (NCDs) were recognized not only as a global health concern but also a threat to social and economic development [1]. Currently, almost 1 million people die from Diabetes and more than 400 million people suffer from it. An accurate detection method of glucose concentration can be an effective way to prevent and treat diabetes [2]. In this way, glucose sensors play an important role in managing the level of blood glucose in diabetic patients.

Two different technologies are nowadays under development for improving glucose sensors, enzymatic and non-enzymatic devices. The former type of glucose test strips has dominated the glucose detection market since the earliest 60s. This biocatalyst provides good selectivity and sensitivity for glucose determination in a self-monitoring application [3]. Three different generations of glucose sensors are currently available. The first-generation glucose sensors depended directly on the available oxygen since this molecule was consumed by the immobilized enzymes for glucose oxidation. In the second-generation auxiliary enzymes are coimmobilized with the analyte converting enzyme to improve the analytical quality and to simplify the performance. Finally, the third generation eliminates the need for a reaction media by enzyme immobilization on the electrode surface, then glucose is oxidized directly by the electrode. However, the second and third generations present problems in terms of electrons transfer and poor reproducibility [4–7].

Some authors report enzyme electrodes with different configurations for glucose detection. Their results present good linear ranges and sensitivity values in accordance with different biological fluids [8,9]. However, it is necessary to overcome barriers such as electrode reusability as long-term sensors will be the commercial leaders in the diabetes market. Attending lifespan criteria, non-enzymatic electrodes present better results than enzymatic-based sensors.

The intrinsic chemical and thermal sensitivity of enzymes have stimulated researchers to explore chemically and thermally stable metal compounds as alternative sensing materials for non-enzymatic glucose detection. This type of sensor forms an oxidation layer, which catalyzes a glucose oxidation reaction, similar to that of the enzyme activity. Various materials such as noble metals, transition metals, and low-cost metals have been considered in this application. Noble metals, although they report good results in terms of linear range and sensitivity, they present major problems related to poisoning, electron transfer kinetics, and poor selectivity [10]. Transition metals and their oxides have gained much attention because of the cost-effectiveness and good catalytic performance for glucose oxidation, in terms of selectivity and sensitivity [11]. The third line of the periodic table of elements contains metals relatively inexpensive and with a rapid and sensitive response toward glucose molecules. Some examples are V, Mn, Fe, Co, Ni, Cu, and Zn [12–14].

In the case of copper, this metal has attracted much attention due to its properties: low cost, several morphologies, good electrocatalytic activity, and high surface area. Copper presents a good electrocatalytic capacity due to Cu^{2+} and Cu^{3+} ions, which act as a redox pair in catalytic processes [15]. The proposed reaction mechanism for glucose oxidation to gluconolactone in basic media is shown below:

$$Cu \rightarrow Cu^{2+} + 2e^{-} \quad (1)$$

$$Cu^{2+} + 2OH^{-} \rightarrow Cu(OH)_2 \quad (2)$$

$$Cu(OH)_2 \rightarrow CuO + H_2O \quad (3)$$

$$CuO + OH^{-} \rightarrow CuOOH + e^{-} \quad (4)$$

$$2CuOOH + glucosa \rightarrow 2CuO + glucolactone + 2H_2O \quad (5)$$

However, the single metal has poor conductivity, which hinders the transport of electrons between the catalyst and the electrode, and thus, it reduces the catalytic performance of the material [16]. Attending to the proposed reaction mechanism, copper oxide provides a more direct glucose oxidation reaction.

In this context, previous works studied the effect of different copper oxide morphologies and nanostructures for glucose detection. Thus, recent studies have proposed nanospheres, nanowires, and nanostrips structures as they provide a larger specific surface area and superior physical and chemical properties [17]. The results reported showed high reproducibility, wide linear ranges, and low detection limits for glucose in alkali media. Different nanostructures have been tested in similar conditions, for example, Pourbeyram et al. reported a copper oxide nanoparticle on a graphene oxide electrode with high sensitivity to glucose and a linear correlation in the range of glucose concentration from 0.1 to 150.0 μM [18]. Wang et al. have synthetized mesoporous CuO electrodes with a sensitivity of 0.08 mA·mM-1 and a linear range of 170–310 μM [19].

To advance the state of the art, this work intends to develop a simple but useful and robust, copper oxide electrode constituting a step forward in low-cost non-enzymatic sensors. After a rigorous characterization for glucose sensing application, the results achieved have been compared with complex copper oxides electrodes in terms of linear range, sensitivity, and stability. Besides these aspects, the effect of common interferences present in the glucose oxidation reaction has been studied.

2. Materials and Methods

This section reports the materials used and the methods employed to the complete characterization of the electrode, paying special attention to developing a synthesis method that can be considered reproducible, effective, and environmentally friendly.

2.1. Apparatus and Chemicals

Copper (II) sulfate pentahydrate (≥99.9%), L-ascorbic acid reagent (99.7%), Ibuprofen (≥98%), Sulfuric acid (≥99.7%), and Nafion TM 117 (5%) were purchased from Sigma-Aldrich Corporation (St. Louis, MO, USA). For its part, D(+)-glucose anhydrous (97%), ethanol (absolute pure), potassium chloride, and sodium hydroxide pellets were purchased from PanReac AppliChem Uric acid (99%) was acquired from Alfa Aesar Chemicals (Haverhill, MA, USA). Finally, Potassium ferrocyanide ($K_4Fe(CN)_6$) and Hexaammineruthenium (III) chloride ($Ru(NH_3)_6Cl_3$) were purchased from Sigma Aldrich. All chemicals were used as received without any further purification. Distilled water (18.2 MU cm) was used in all experiments to prepare all solutions and was purified with the Millipore Advantage A10 water system.

The carbon and gold-based screen-printed electrodes with a visual area of 0.12 cm^2 were purchased from Metrohm Dropsens. All measurements were performed with PalmSens 4 potentiostat, galvanostat, impedance analyzer. The apparatus has a large potential range (−10 V to 10 V) and a current range (100 pA to 10 mA) with a high resolution and low noise. PSTrace 7 software collects and displays the measurements for the glucose detection electrodes. The schematics of the experimental setup are shown in Figure 1.

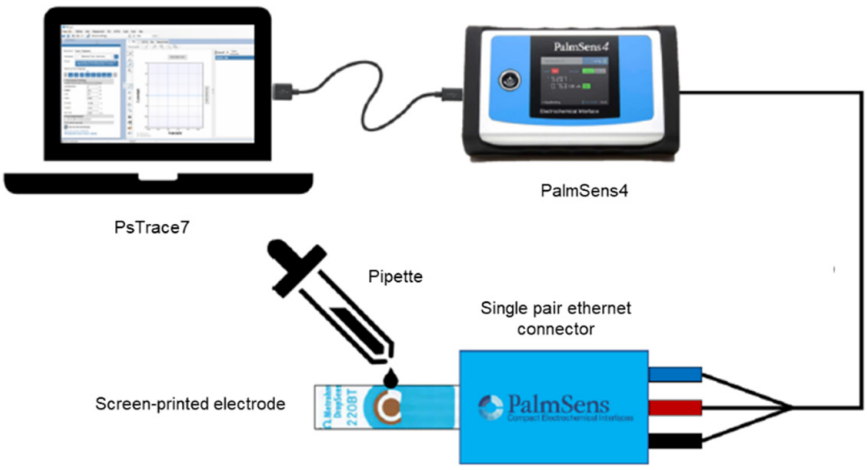

Figure 1. Experimental set-up.

2.2. Electrodeposition of Cu and CuO

The preparation of the working electrode consists of the reconditioning of the carbon screen-printed electrode by washing with distilled water and immediately afterward with pure ethanol. The electrode surface is then dried at ambient conditions. Before the electrodeposition of copper particles, the cleaned surface is treated with two cyclic voltamperometries techniques in the range of −0.6 V to 0.6 V vs. Ag/AgCl at a scan rate of 100 mV/s with 0.1 M $CuSO_4$ $5H_2O$ and 0.1 M H_2SO_4. The solution is deposited onto the electrode surface with the corresponding pipette.

Cu particles are electrodeposited by chemical reduction of 0.1 M $CuSO_4$ $5H_2O$ in 0.1 M H_2SO_4 using the chronoamperometry technique at −0.366 V vs. Ag/AgCl according to previous studies [20]. The deposition time of Cu particles on the carbon-printed electrode (CPE) was studied from 100 s to 800 s.

For the oxidation of copper particles, 20 voltammetry cycles from −0.5 V to 0.5 V vs. Ag/AgCl at a scan rate of 100 mV/s with 1 M NaOH solution is needed. Figure 2 compares the electrode before and after.

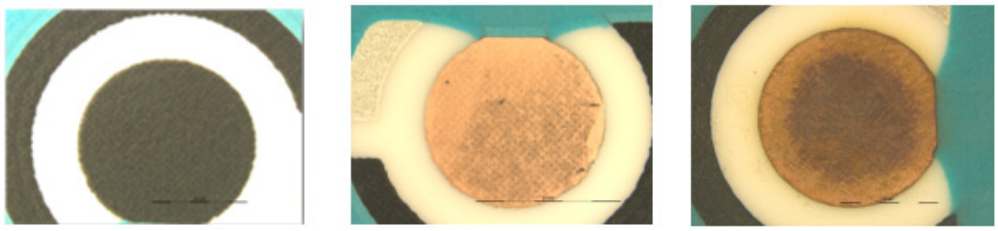

(**a**) (**b**) (**c**)

Figure 2. Screen-printed electrodes (**a**) carbon printed electrode—before copper electrodeposition; (**b**) copper-based electrode—before oxidation step; (**c**) copper oxide electrode.

2.3. Electrode Characterization and Electrochemistry Measurements

The electrode characterization is addressed by scanning electron microscopy (SEM) and Energy X-ray Powder Diffraction analysis with the SEM microscopy EVO MA15 ZEISS ® (Germany). The morphology of the electrode surface after the galvanostatic electrodeposition was studied by recording SEM images.

For the electrochemical behavior of the electrode, several techniques were used. Cyclic voltammetry displays the redox reaction profiles, and therefore the glucose oxidation potential can be determined for the different metallic microstructures. To mimic a real application of a continuous glucose sensor, chronoamperometry and pulsed amperometry detection techniques are mostly employed. A constant potential is applied while the glucose is oxidized onto the electrode surface.

3. Results and Discussion

This section reports and discusses the main results accomplished for the development of the new non-enzymatic amperometric glucose screen-printed sensor.

3.1. Characterization of Screen-Printed Electrodes Modified with Copper and Copper Oxide Particles

Figure 3 depicts the SEM morphology of the synthesized sensors. The image shows the presence of copper and copper oxide particles on carbon surfaces. The particle size for copper and copper oxide is 2 µm, but particle agglomeration was more present in the case of copper-based electrodes. The size is in accordance with previous articles and promotes a high increment in the electrode surface area [20]. The particles were homogeneously dispersed as shown by the white dots on both images (Figure 3a,b). Figure S1 in the Supplementary Materials shows the rough surface of carbon screen printed electrodes, where the copper microparticles are electrodeposited.

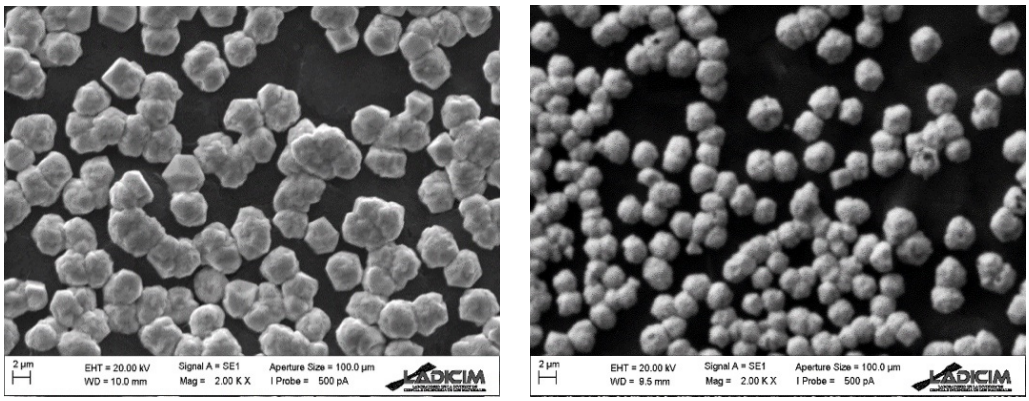

(**a**) (**b**)

Figure 3. SEM image of copper and copper oxide-based electrodes: (**a**) copper-based electrode; (**b**) copper oxide electrode.

The composition of both electrodes was analyzed by using Energy X-ray Powder Diffraction (EDX). Figure 4. illustrates the spectrum for the copper and copper oxide profiles. As it is shown in Figure 4 copper was present in both electrodes in more than 50% in terms of weight percentage, 71% for copper-based electrode and 57% for copper oxide electrode. Up to 30% of the weight of copper oxide corresponds to oxygen, while in the case of copper-based electrodes the percentage is only 5%. These results are in good agreement with previously reported results in the literature [21]. Sun et al., performed an electrode composed of CuO spindle-like nanosheets grown on a carbon cloth [22].

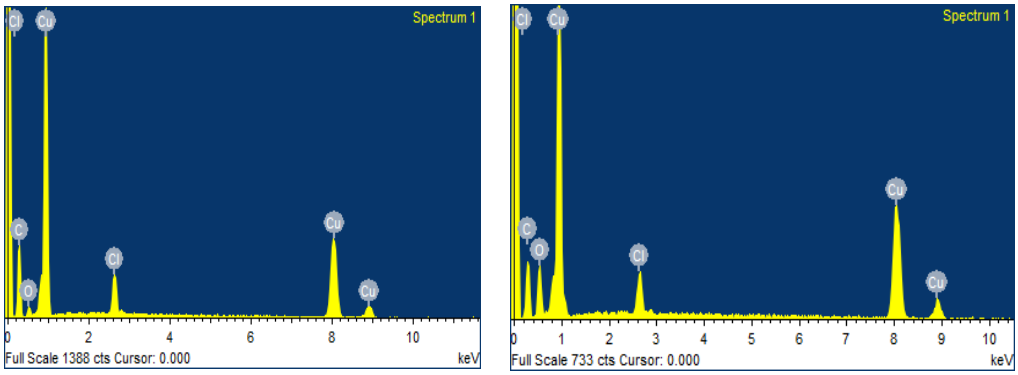

(**a**) (**b**)

Figure 4. EDX spectra of copper and copper oxide-based electrodes: (**a**) copper-based electrode; (**b**) copper oxide electrode.

The electroactive area of the electrode was estimated from cyclic voltammetry performed at different scan rates. Commercial gold, copper, and copper oxide particles' active areas were compared by using different reactants, $[Ru(NH_3)_6]^{3+}$ and $[Fe(CN)_6]^{4-}$. These species follow the next reactions when the potential is applied on the electrode surface [23,24]:

$$[Ru(NH_3)_6]3^+ + e^- \leftrightarrow [Ru(NH_3)_6]2^+ \quad (6)$$

$$[Fe(CN)_6]3^- + e^- \leftrightarrow [Fe(CN)_6]4^- \quad (7)$$

Peak to peak separation (ΔEp) analysis of the cyclic voltammetry profiles is useful to determine if the redox process is reversible or irreversible. For those cases where ΔEp—57 mV and is independent of the scan rate, the process is considered reversible. On the contrary, when ΔEp increases with the scan rate, the redox process is classified as quasi- or irreversible.

In the latter case, the Randles Equation (Equation (8)) can be applied. This equation relates the effect of scan rate on the current peak.

$$i_p = 0.4463 \cdot \left(\frac{F^3}{RT}\right) \cdot n^{3/2} \cdot A \cdot C \cdot D^{1/2} \cdot v^{1/2} \quad (8)$$

where F is Faraday constant (96,500 C mol^{-1}), R is the universal gas constant (8143 J mol^{-1} K^{-1}) and T is the absolute temperature (K). The other parameters are: n, number of electrons involved in the redox half-reaction (-); D, the diffusion coefficient for the redox-active species on the solution media (cm^2 s^{-1}), C is the solution molar concentration of the redox species (mol cm^{-3}) and A is the surface area (cm^2) and v is the scan rate of the experiment (V s^{-1}).

The Randles–Ševčík equation is often written in an abbreviated form under the assumption that the temperature is fixed at 298.15 K (25 °C) [25]. For this specific temperature, the constants appearing at the beginning of the equation, 0.4463, can be combined allowing the equation to be written in a simplified form as follows [25]:

$$i_p = \left(2.99 \times 10^5\right) \cdot n^{3/2} \cdot A \cdot C \cdot D^{1/2} \cdot v^{1/2} \quad (9)$$

The constant appearing at the beginning of this simplified equation, 2.99×10^5 is known to have units $C\ mol^{-1}\ v^{-1/2}$.

For gold-based electrodes, 1 mM $K_4Fe(CN)_6$ in 0.1 M KCl was used as redox solution for active area determination. The scan rate varies from 100 to 10 mV s^{-1}. Diffusion coefficient of $K_4Fe(CN)_6$ in 0.1 M KCl were obtained from Pahlavi et al., which reported a value of 7.6×10^{-6} $cm^2\ s^{-1}$ [26].

Figure 5 shows cyclic voltammetry profiles and Randles Equation linear regression for gold-based electrodes. As expected gold commercial visual area coincided with the active area determined by the Randles–Ševčík equation, 0.12 cm^2. This result demonstrates that there are no significant nanostructures that contribute to increasing the surface area of the commercial electrode. The experiment was repeated twice obtaining the same result, no variation between visual and active area.

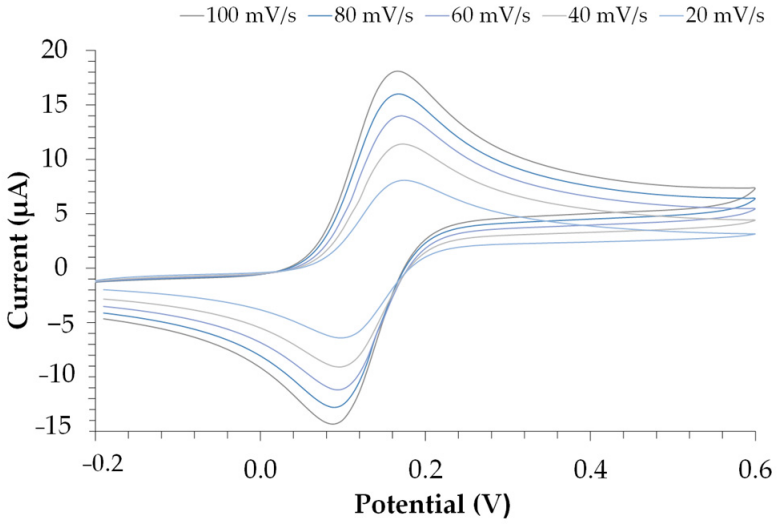

(**a**)

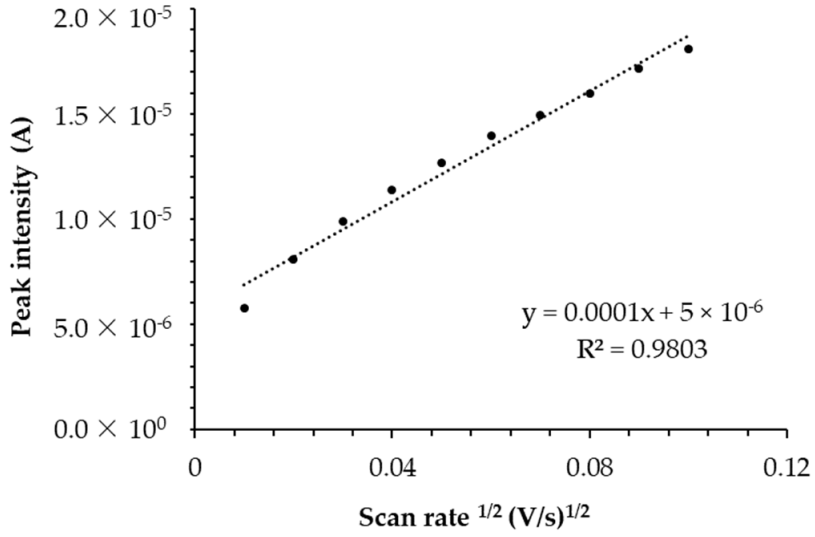

(**b**)

Figure 5. Active area calculation for the gold commercial-based electrode: (**a**) Cyclic voltammetry with 1 mM $K_4Fe(CN)_6$ in 0.1 M KCl with a scan rate from 100 to 10 mV s^{-1}; (**b**) Randles Equation linear regression.

Selecting the correct probe is crucial to gain accuracy in calculating the active area of the electrode. For copper-based electrodes, $K_4Fe(CN)_6$ is not recommended because iron ions interact with copper atoms leading to unstable cyclic voltammetry profiles, therefore different probes should be used. In this work, $[Ru(NH_3)_6]^{3+}$ salt has been selected for the characterization of the active area of copper-based electrodes. In this case, the diffusion coefficient of 5 mM $Ru(NH_3)_6Cl_3$ in 0.1 M KCl was obtained from Lee et al. which reported a value of 8.43×10^{-6} cm^2 s^{-1} [24].

Cyclic voltammetry experiment displayed from 500 mV s^{-1} to 10 mVs^{-1} also was used to determine the active area by the Randles–Ševčík equation. In this case, the surface area was increased from 0.12 cm^2 to 1.72 cm^2. Considering all the experiments, the error is less than 15%. Figure S2 represents the cyclic voltammetry experiment for copper-based electrode and the linear fitting to the Randles–Ševčík equation (Equation (9)).

$Ru(NH_3)_6Cl_3$ was also used for the determination of the copper oxide active area. The experimental conditions were the same as in the determination of the copper active area. In this case, the active area was 1.50 cm^2. Figure S3 represents the cyclic voltammetry experiment for a copper oxide electrode. Considering other tested electrodes, the average active area was 1.6 ± 0.2 cm^2.

3.2. Electrooxidation of Glucose

The oxidation mechanism of glucose was firstly studied by using cyclic voltammetry. Figure 6 represents the cyclic voltammetry profile of the commercial gold, copper, and copper oxide electrodes. All electrodes were conditioned with cyclic voltammetry with 0.1 M NaOH before use.

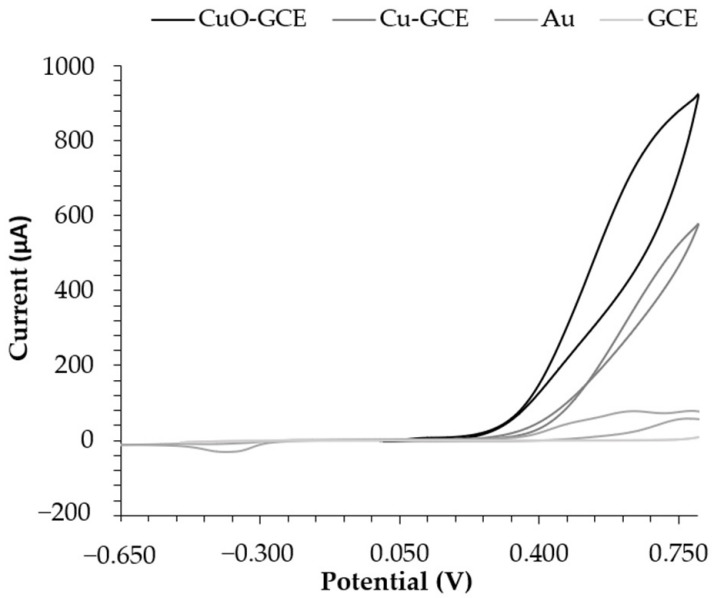

Figure 6. Cyclic voltammetry (1 cycle, −0.00 to 0.85 V vs. Ag/AgCl) with 5 mM glucose in 0.1 M NaOH with copper, copper oxide gold, and glassy carbon electrode.

As it can be seen in Figure 6, copper oxide provides a higher amperometric signal when 5 mM glucose is oxidized in basic media. CuO is directly oxidized to CuOOH, a strong oxidizing agent. The Cu (III) species then electrochemically oxidized glucose to gluconolactone, responding to the oxidation peak of glucose's oxidation reaction, as shown in Figure 6. In the case of copper, this metal needs to be oxidized to Cu (III) in two reaction steps. In the case of gold and bare carbon, they do not present significant catalytic activity for glucose oxidation.

Cyclic voltammetry was also employed to determine glucose in different concentrations using the reported electrodes as the working electrode. Based on the cyclic voltammetry profiles in Figure 6, the glucose oxidation potential is fixed in 0.55 V. Figure S4

represents cyclic voltammetries for a copper oxide electrode from 1 to 10 mM of glucose. These data were used to determine the calibration curve of the electrode.

All experiments were replicated three times keeping the same conditions: temperature, pH, cycles voltage, and conditioning process. The calibration curves in Figure 7 show a linear range of up to 5 mM of glucose in all cases. For copper oxide electrode, the linear equation is y (μA) = 108.48 × (mM) + 8.59 with a regression coefficient of 0.99. In the case of copper, the equation is y (μA) = 54.65 × (mM) + 36.06. The gold commercial electrode does not show a significant sensitivity for glucose.

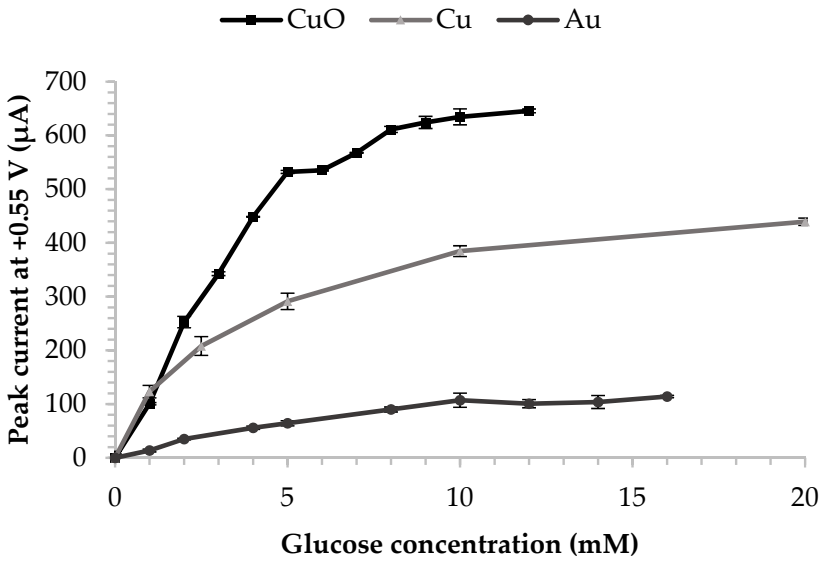

Figure 7. Calibration curve of current response vs. glucose concentration for copper oxide, copper, and commercial gold electrode.

The amperometric signal starts to decline because the active surface of the electrode is saturated with glucose. The sensitivity reported in the linear ranges is 904 $\mu A \cdot mM^{-1} \cdot cm^{-2}$. The limit of detection (LOD) was 0.002 mM, it was estimated by using (Equation (10)):

$$LOD = 3.3 \cdot \frac{s_y}{S} \quad (10)$$

where S_y is the standard deviation of the regression line and S is the slope.

Blood and interstitial fluid normal glucose values go from 4 mM to 11 mM of glucose [27,28]. However, other biological fluids present glucose maximum values lower than 5 mM, this is the case of pleural, ascites, and spinal liquid besides urine and tears [29–33].

Table 1 shows results from similar non-enzymatic electrodes. The developed copper oxide electrode provides good linearity and high sensitivity compared to similar electrodes reported in literature.

Table 1. Copper and copper oxide-based electrodes for glucose sensing.

Electrode	Linear Range (mM)	LOD (μM)	Sensitivity ($\mu A \cdot mM^{-1} \cdot cm^{-2}$)	Media NaOH	Ref
Cu/Graphene	0.02–2.3	1.39	379.71	0.1 M	[34]
Cu_2O	0.05–6.0	0.13	277.1	0.1 M	[35]
Cu/Polyaniline/Graphene	0.001–3.7	0.27	150	0.1 M	[36]
CuO/NC [1]	0.0001–2.55	0.14	272.6	0.1 M	[37]
CuO/GCE	0.005–5.89	0.012	1467.32	0.1 M	[38]
CuO/stainless	0–3	N/A	1017	0.1 M	[21]
CuO/GCE	0–5	0.002	904	0.1 M	This work

[1] NC = nanocomposite.

3.2.1. Reproducibility, Repeatability, and Stability

Copper oxide electrodes were also characterized in terms of reproducibility among different electrodes, repeatability, and stability with time for different storage conditions: NaOH 0.1 M, distilled water, and ambient conditions.

Measurements from nine different electrodes with different glucose concentrations are represented in Figure 8. The variation among the electrodes is attributed to the variability of the active area. Error bars corresponding to error less than 18% in the worst case. All measurements were performed under basic media with cyclic voltammetry electrochemical technique. Data were collected at 0.55 V vs. Ag/AgCl.

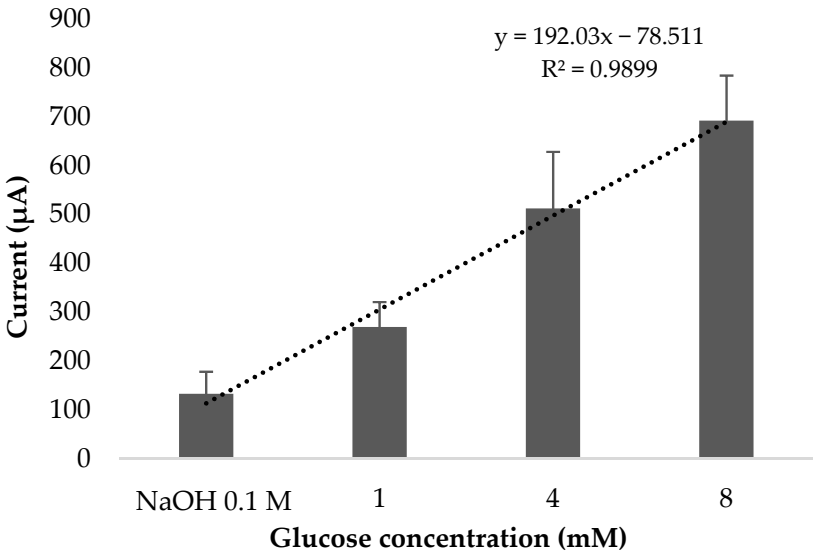

Figure 8. Reproducibility of copper oxide electrode. Data from 9 copper oxide electrodes synthesized with the same protocol and conditions.

Regarding repeatability, there is no significant variability among measurements within the same copper oxide electrode. For this experiment, a glucose concentration of 4 mM was measured up to 25 times with the same electrode. As it can be seen in Figure 9, all profiles coincide pointing to good repeatability of the copper oxide electrode. Not all measurements are represented in the chart below.

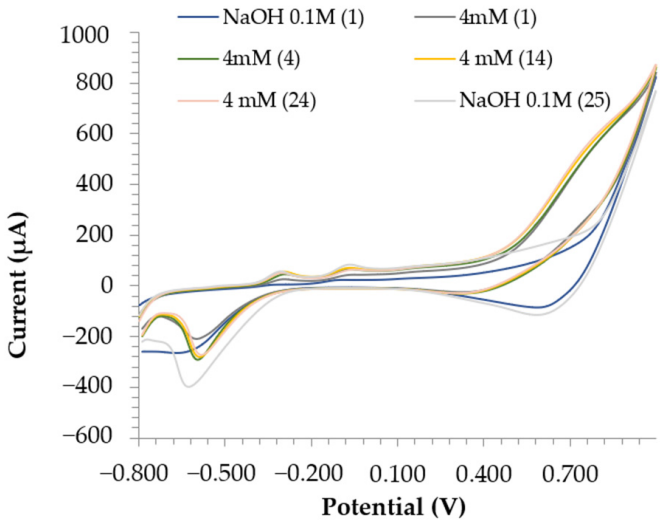

Figure 9. Repeatability of copper oxide electrode. 25 measurements of 4 mM of glucose in 0.1 M NaOH. (x) refers to electrode measurement repetition number.

A pulsed amperometric detection technique was employed to determine the stability through time. This electrochemical technique uses a fixed potential to measure glucose concentration in a bulk solution. The fixed potential was set to +0.55 V according to previous experiments. Figure 10 shows 3 days measurements for the same copper oxide electrode. A total number of 120 measurements were performed every day.

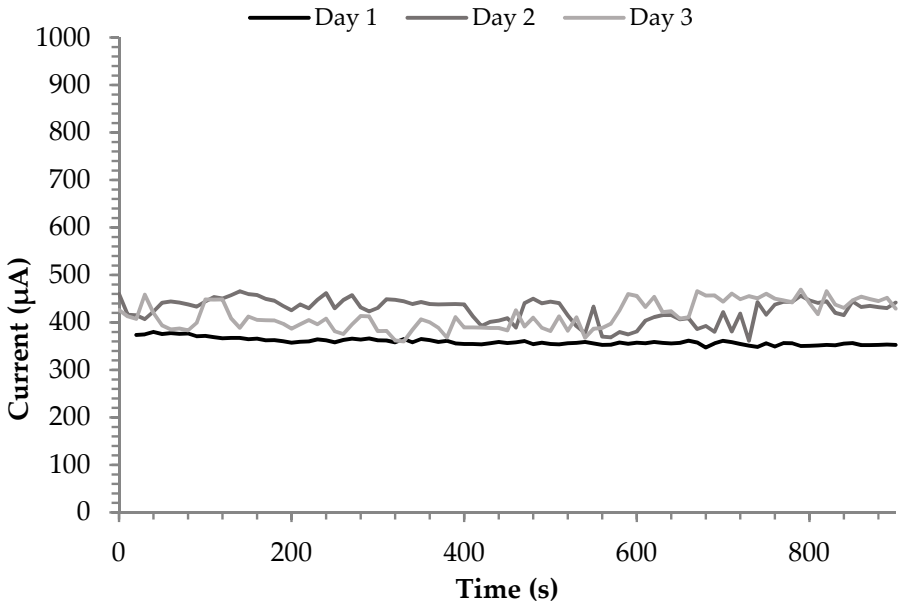

Figure 10. Stability of copper oxide electrode. Pulsed amperometric detection (+0.55V) of 4 mM glucose in 0.1 M NaOH during 1200 measurements each 10 s.

For the first day, the signal for 4 mM is slightly smaller than the one obtained with cyclic voltammetry. However, its value remains constant at 360 ± 7 μA for 1000 s. For the second and third day, the signal increased up to 426 and 416 μA, respectively. However, the error percentage also increased to 6% in both cases. This signal increase could represent a higher copper oxide/copper ratio due to the surface contact with the atmospheric oxygen.

Considering the electrode sensitivity, 904 μA $mmol^{-1}$ L^{-1} cm^{-2}, this increase represents a 12.5% over the concentration of the study (4 mM of glucose).

3.2.2. Common Interferences Study

Another important aspect of a good glucose sensor is the performance in the presence of common interferences. Most of the nonenzymatic glucose sensors based on precious metals and alloys present poison problems in presence of chloride ions [39]. Other molecules such as ibuprofen (IB), ascorbic (AA), and uric acid (UA) were also investigated since they are glucose coexisting species in common biological fluids. Concentration values for the analysis have been selected according to the maximum biological values in the bloodstream [40–42].

Figure 11 represents the electrode signal for 4 mM of glucose with and without the interferences of 0.41 mM UA and 0.05 mM of IB. At 300 s, the bulk solution—4 mM of glucose and the corresponding interference concentration—was changed to the 4 mM glucose solution. As it can be seen in Figure 11, the presence of 0.41 mM UA decreases the electrode signal roughly by 16%, which according to the reported sensitivity, this means a variation of 0.46 mM. It is hypothesized that uric acid may be adsorbed onto the electrode surface blocking glucose to be oxidized. However, the signal reduction meets the commercial error requirements.

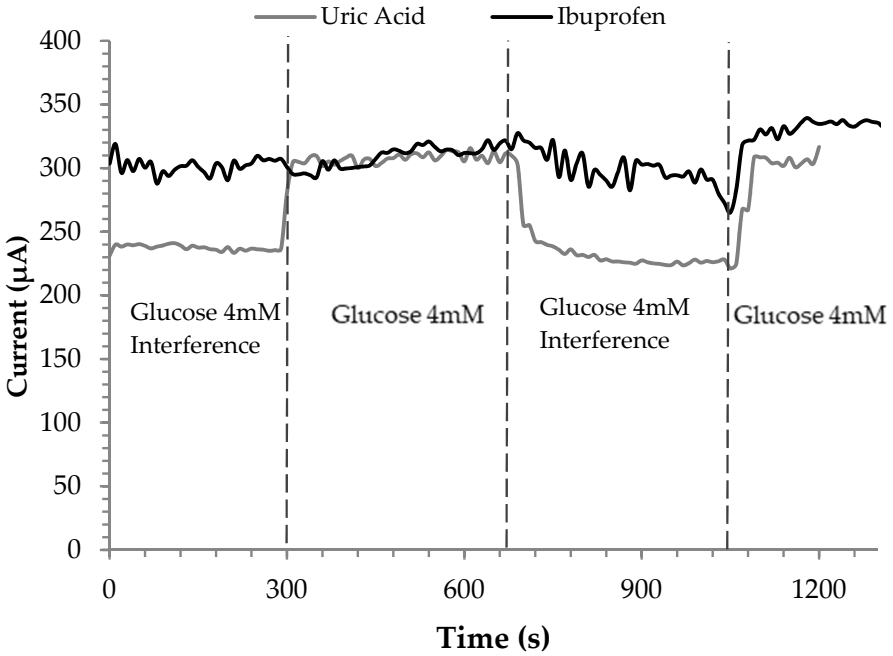

Figure 11. Pulsed Amperometric response of the copper oxide electrode in the presence of common interfering substances and 4 mM of glucose at +0.55 V (vs. Ag/AgCl) in 0.1M NaOH (pH 13). 0.41 mM uric acid and 0.05 mM ibuprofen.

On the other side, ibuprofen does not interfere the glucose oxidation on copper oxide electrodes.

Figure 12 shows the signal with chlorine and ascorbic acid interferences. This time the experiment started with 4 mM glucose solution and after 340 s, the bulk solution was replaced by a solution of glucose and the respective interference.

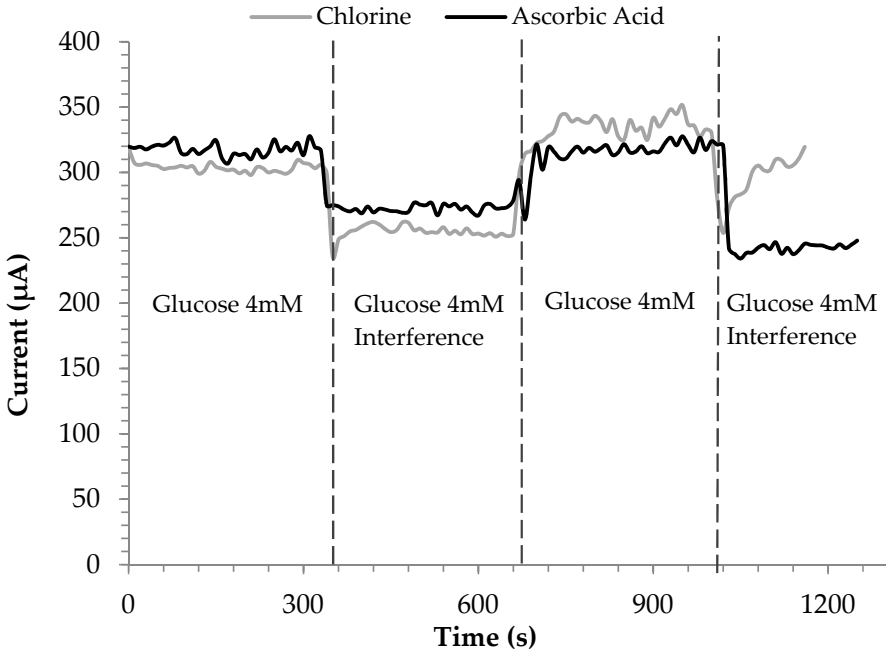

Figure 12. Pulsed Amperometric response of the copper oxide electrode in the presence of common interfering substances and 4 mM of glucose at +0.55 V (vs. Ag/AgCl) in 0.1 M NaOH (pH 13). 0.1 mM ascorbic acid and 0.1 M chlorine.

Chlorine reduced the electrode signal up to 15% while ascorbic acid reduced it by nearly 14%. This result indicates that CuO/GCE relatively prevented the poisoning of the chloride ion, which made some nonenzymatic glucose sensors lose their activity.

All interferences, except ibuprofen, decrease the glucose oxidation signal by less than 18%. It means that the interfering molecule is adsorbed on the active sites of the electrode blocking the area for the glucose to be oxidized. However, the signal reduction fits the standard error provided by ISO 15197.

4. Conclusions

In this study, the electrode made by CuO was successfully synthesized on a carbon printed electrode. The reported protocol provided reproducible and good results in terms of sensitivity, stability, and linear range up to 5 mM. In addition, the electrode response, independently of common biological interferences, meet the ISO requirements for in vitro glucose diagnostic self-test systems.

This work opens up new opportunities for constructing nanostructure material for high-performance and affordable non-enzymatic glucose sensors. More efforts are still needed for the development of electrodes sensitive to physiological conditions, especially pH.

Supplementary Materials: The following are available online at https://www.mdpi.com/article/10.3390/app112210830/s1, Figure S1: SEM image of carbon screen printed microelectrodes. (a) 200×. (b) 2000×, Figure S2: Active area calculation for copper based electrode (a) Cyclic voltam-metry with 5 mM $Cl_3[Ru(NH_3)_6]$ in 0.1 M KCl with a scan rate from 500 to 10 mV s^{-1}. (b) Randles-Equation linear regression. Figure S3: Active area calculation for copper oxide based electrode (a) Cyclic voltammetry with 5 mM $Cl_3[Ru(NH_3)_6]$ in 0.1 M KCl with a scan rate from 500 to 10 mV s^{-1}. (b) Randles-Equation linear regression. Figure S4: Copper oxide electrode cyclic voltammetry curves (1 cycle, −0.7 to +0.7 V vs. Ag/AgCl) with different glucose concentrations in 0.1 M NaOH.

Author Contributions: Conceptualization, C.G. and L.G.-C.; methodology, C.G., L.G.-C. and M.F.; formal analysis, C.G.; investigation, C.G.; data curation, C.G.; writing—original draft preparation, C.G.; writing—review and editing, C.G., L.G.-C., M.F. and I.O.; supervision, I.O.; funding acquisition, I.O. All authors have read and agreed to the published version of the manuscript.

Funding: This research was funded by the Spanish Ministry of Science, Innovation, and Universities under the project RTI2018-093310-B-I00, grant Concepción Arenal from the University of Cantabria.

Data Availability Statement: Data available on request.

Acknowledgments: Financial support from the Spanish Ministry of Science, Innovation, and Universities under the project RTI2018-093310-B-I00 is gratefully acknowledged. Carlota Guati also is grateful to the Concepción Arenal postgraduate research grant from the University of Cantabria.

Conflicts of Interest: The authors declare no conflict of interest.

References

1. United Nations. ODS 3 Good Health. Available online: https://www.un.org/sustainabledevelopment/health/ (accessed on 5 July 2021).
2. Chen, H.; Fan, G.; Zhao, J.; Qiu, M.; Sun, P.; Fu, Y.; Han, D.; Cui, G. A portable micro glucose sensor based on copper-based nanocomposite structure. *New J. Chem.* **2019**, *43*, 7806–7813. [CrossRef]
3. Lee, H.; Hong, Y.J.; Baik, S.; Hyeon, T.; Kim, D.H. Enzyme-Based Glucose Sensor: From Invasive to Wearable Device. *Adv. Healthc. Mater.* **2018**, *7*, 1701150. [CrossRef]
4. Hassan, I.U.; Salim, H.; Naikoo, G.A.; Awan, T.; Dar, R.A.; Arshad, F.; Tabidi, M.A.; Das, R.; Ahmed, W.; Asiri, A.M.; et al. A review on recent advances in hierarchically porous metal and metal oxide nanostructures as electrode materials for supercapacitors and non-enzymatic glucose sensors. *J. Saudi Chem. Soc.* **2021**, *25*, 101228. [CrossRef]
5. Long, L.; Liu, X.; Chen, L.; Li, D.; Jia, J. A hollow CuOx/NiOy nanocomposite for amperometric and non-enzymatic sensing of glucose and hydrogen peroxide. *Microchim. Acta* **2019**, *186*, 5–10. [CrossRef]
6. Veeramani, V.; Madhu, R.; Chen, S.M.; Veerakumar, P.; Hung, C.T.; Liu, S. Bin Heteroatom-enriched porous carbon/nickel oxide nanocomposites as enzyme-free highly sensitive sensors for detection of glucose. *Sens. Actuators B Chem.* **2015**, *221*, 1384–1390. [CrossRef]

7. Madhu, R.; Veeramani, V.; Chen, S.M.; Manikandan, A.; Lo, A.Y.; Chueh, Y.L. Honeycomb-like Porous Carbon-Cobalt Oxide Nanocomposite for High-Performance Enzymeless Glucose Sensor and Supercapacitor Applications. *ACS Appl. Mater. Interfaces* **2015**, *7*, 15812–15820. [CrossRef]
8. Gonzalez-Solino, C.; Bernalte, E.; Bayona Royo, C.; Bennett, R.; Leech, D.; Di Lorenzo, M. Self-Powered Detection of Glucose by Enzymatic Glucose/Oxygen Fuel Cells on Printed Circuit Boards. *ACS Appl. Mater. Interfaces* **2021**, *13*, 26704–26711. [CrossRef]
9. Liang, H.; Wang, L.; Yang, Y.; Song, Y.; Wang, L. A novel biosensor based on multienzyme microcapsules constructed from covalent-organic framework. *Biosens. Bioelectron.* **2021**, *193*, 113553. [CrossRef]
10. Hwang, D.W.; Lee, S.; Seo, M.; Chung, T.D. Recent advances in electrochemical non-enzymatic glucose sensors—A review. *Anal. Chim. Acta* **2018**, *1033*, 1–34. [CrossRef]
11. Niu, X.; Li, X.; Pan, J.; He, Y.; Qiu, F.; Yan, Y. Recent advances in non-enzymatic electrochemical glucose sensors based on non-precious transition metal materials: Opportunities and challenges. *RSC Adv.* **2016**, *6*, 84893–84905. [CrossRef]
12. Pathak, D.K.; Chaudhary, A.; Tanwar, M.; Goutam, U.K.; Mondal, P.; Kumar, R. Nickel Cobalt Oxide Nanoneedles for Electrochromic Glucose Sensors. *ACS Appl. Nano Mater.* **2021**, *4*, 2143–2152. [CrossRef]
13. Lakhdari, D.; Guittoum, A.; Benbrahim, N.; Belgherbi, O.; Berkani, M.; Vasseghian, Y.; Lakhdari, N. A novel non-enzymatic glucose sensor based on NiFe(NPs)—Polyaniline hybrid materials. *Food Chem. Toxicol.* **2021**, *151*, 112099. [CrossRef]
14. Jadhav, S.B.; Malavekar, D.B.; Kale, S.B.; Sabale, S.R.; Patil, U.M.; Lokhande, C.D.; Pawaskar, P.N. Reliable glucose sensing properties of electrodeposited vertically aligned manganese oxide thin film electrode. *Appl. Phys. A Mater. Sci. Process.* **2021**, *127*, 1–9. [CrossRef]
15. Sehit, E.; Altintas, Z. Significance of nanomaterials in electrochemical glucose sensors: An updated review (2016–2020). *Biosens. Bioelectron.* **2020**, *159*, 112165. [CrossRef] [PubMed]
16. Xu, K.; Ding, H.; Lv, H.; Chen, P.; Lu, X.; Cheng, H.; Zhou, T.; Liu, S.; Wu, X.; Wu, C.; et al. Dual Electrical-Behavior Regulation on Electrocatalysts Realizing Enhanced Electrochemical Water Oxidation. *Adv. Mater.* **2016**, *28*, 3326–3332. [CrossRef] [PubMed]
17. Zhou, Q.; Zhang, Y.; Zeng, T.; Wan, Q.; Yang, N. Morphology-dependent sensing performance of CuO nanomaterials. *Anal. Chim. Acta* **2021**, *1171*, 338663. [CrossRef] [PubMed]
18. Pourbeyram, S.; Abdollahpour, J.; Soltanpour, M. Green synthesis of copper oxide nanoparticles decorated reduced graphene oxide for high sensitive detection of glucose. *Mater. Sci. Eng. C* **2019**, *94*, 850–857. [CrossRef] [PubMed]
19. Wang, M.F.; Huang, Q.A.; Li, X.Z.; Wei, Y. Mesoporous CuO: Alternative enzyme-free glucose sensing structure with excellent kinetics of electrode process. *Anal. Methods* **2012**, *4*, 3174–3179. [CrossRef]
20. Nurani, D.A.; Wibowo, R.; Fajri, I.F. El Non-enzymatic glucose sensor based on electrodeposited copper on carbon paste electrode (Cu/CPE). *AIP Conf. Proc.* **2016**, *1729*, 020056. [CrossRef]
21. Patil, A.S.; Patil, R.T.; Lohar, G.M.; Fulari, V.J. Facile synthesis of CuO nanostructures for non-enzymatic glucose sensor by modified SILAR method. *Appl. Phys. A Mater. Sci. Process.* **2021**, *127*, 101. [CrossRef]
22. Sun, S.; Shi, N.; Zhang, B.; Liao, X.; Huang, Z.; Chen, X.; Pu, X.; Yin, G. Hierarchically porous CuO spindle-like nanosheets grown on a carbon cloth for sensitive non-enzymatic glucose sensoring. *Nanotechnology* **2020**, *31*, 375502. [CrossRef] [PubMed]
23. Pérez-Fernández, B.; Martín-Yerga, D.; Costa-García, A. Galvanostatic electrodeposition of copper nanoparticles on screen-printed carbon electrodes and their application for reducing sugars determination. *Talanta* **2017**, *175*, 108–113. [CrossRef]
24. Lee, J.; Arrigan, D.W.M.; Silvester, D.S. Mechanical polishing as an improved surface treatment for platinum screen-printed electrodes. *Sens. Bio-Sens. Res.* **2016**, *9*, 38–44. [CrossRef]
25. Ferrari, A.G.M.; Foster, C.W.; Kelly, P.J.; Brownson, D.A.C.; Banks, C.E. Determination of the electrochemical area of screen-printed electrochemical sensing platforms. *Biosensors* **2018**, *8*, 53. [CrossRef] [PubMed]
26. Pahlavan, A.; Gupta, V.K.; Sanati, A.L.; Karimi, F.; Yoosefian, M.; Ghadami, M. ZnO/CNTs nanocomposite/ionic liquid carbon paste electrode for determination of noradrenaline in human samples. *Electrochim. Acta* **2014**, *123*, 456–462. [CrossRef]
27. Glucose Blood Levels. Available online: https://www.diabetes.co.uk/diabetes_care/blood-sug (accessed on 4 March 2021).
28. Cengiz, E.; Tamborlane, W.V. A tale of two compartments: Interstitial versus blood glucose monitoring. *Diabetes Technol. Ther.* **2009**, *11*, S-11–S-16. [CrossRef]
29. Julián-Jiménez, A.; Morales-Casado, M.I. Usefulness of blood and cerebrospinal fluid laboratory testing to predict bacterial meningitis in the emergency department. *Neurologia* **2019**, *34*, 105–113. [CrossRef]
30. Huang, L.L.; Xia, H.H.X.; Zhu, S.L. Ascitic fluid analysis in the differential diagnosis of ascites: Focus on cirrhotic ascites. *J. Clin. Transl. Hepatol.* **2014**, *2*, 58–64. [CrossRef] [PubMed]
31. Fitzgerald, D.B.; Leong, S.L.; Budgeon, C.A.; Murray, K.; Rosenstengal, A.; Smith, N.A.; Bielsa, S.; Clive, A.O.; Maskell, N.A.; Porcel, J.M.; et al. Relationship of pleural fluid pH and glucose: A multi-centre study of 2,971 cases. *J. Thorac. Dis.* **2019**, *11*, 123–130. [CrossRef]
32. UCSF Health Glucose Urine Test. Available online: ww.ucsfhealth.org/medical-tests/glucose (accessed on 21 January 2020).
33. Chu, M.X.; Miyajima, K.; Takahashi, D.; Arakawa, T.; Sano, K.; Sawada, S.I.; Kudo, H.; Iwasaki, Y.; Akiyoshi, K.; Mochizuki, M.; et al. Soft contact lens biosensor for in situ monitoring of tear glucose as non-invasive blood sugar assessment. *Talanta* **2011**, *83*, 960–965. [CrossRef] [PubMed]
34. Wang, S.; Zhao, L.; Xu, R.; Ma, Y.; Ma, L. Facile fabrication of biosensors based on Cu nanoparticles modified as-grown CVD graphene for non-enzymatic glucose sensing. *J. Electroanal. Chem.* **2019**, *853*, 113527. [CrossRef]

35. Zhang, F.; Wang, Y.; Wu, X.; Zhang, H.; Huang, S.; Yang, Y.; Xie, A.; Wang, M. Cu_2O hollow microspheres as electrode materials for non-enzymatic electrochemical detection of glucose. *Micro Nano Lett.* **2020**, *15*, 1071–1074. [CrossRef]
36. Shabnam, L.; Faisal, S.N.; Roy, A.K.; Haque, E.; Minett, A.I.; Gomes, V.G. Doped graphene/Cu nanocomposite: A high sensitivity non-enzymatic glucose sensor for food. *Food Chem.* **2017**, *221*, 751–759. [CrossRef]
37. Vediyappan, V.; Sivakumar, M.; Chen, S.M.; Lai, Q.; Madhu, R. Nanolayers of carbon protected copper oxide nanocomposite for high performance energy storage and non-enzymatic glucose sensor. *J. Alloys Compd.* **2021**, *875*, 160063. [CrossRef]
38. Ahmad, R.; Khan, M.; Mishra, P.; Jahan, N.; Ahsan, M.A.; Ahmad, I.; Khan, M.R.; Watanabe, Y.; Syed, M.A.; Furukawa, H.; et al. Engineered Hierarchical CuO Nanoleaves Based Electrochemical Nonenzymatic Biosensor for Glucose Detection. *J. Electrochem. Soc.* **2021**, *168*, 017501. [CrossRef]
39. Cherevko, S.; Chung, C.H. The porous CuO electrode fabricated by hydrogen bubble evolution and its application to highly sensitive non-enzymatic glucose detection. *Talanta* **2010**, *80*, 1371–1377. [CrossRef] [PubMed]
40. Mehlisch, D.R.; Sykes, J. Ibuprofen blood plasma levels and onset of analgesia. *Int. J. Clin. Pract. Suppl.* **2013**, *67*, 3–8. [CrossRef] [PubMed]
41. Chemocare Uric Acid Blood Levels. Available online: https://chemocare.com/chemotherapy/side-effects/hy (accessed on 15 July 2021).
42. Mayo Clinic Laboratories Ascorbic Acid Blood Levels. Available online: https://www.mayocliniclabs.com/test-catalog/Clinic (accessed on 15 July 2021).